

# An energy- and charge-conserving, nonlinearly implicit, electromagnetic 1D-3V Vlasov-Darwin particle-in-cell algorithm

G. Chen<sup>a,\*</sup>, L. Chacón<sup>a</sup>

<sup>a</sup>*Los Alamos National Laboratory, Los Alamos, NM 87545*

---

## Abstract

A recent proof-of-principle study proposes a nonlinear electrostatic implicit particle-in-cell (PIC) algorithm in one dimension (Chen, Chacón, Barnes, *J. Comput. Phys.* **230** (2011) 7018). The algorithm employs a kinetically enslaved Jacobian-free Newton-Krylov (JFNK) method, and conserves energy and charge to numerical round-off. In this study, we generalize the method to electromagnetic simulations in 1D using the Darwin approximation of Maxwell's equations, which avoids radiative aliasing noise issues by ordering out the light wave. An implicit, orbit-averaged time-space-centered finite difference scheme is applied to both the 1D Darwin field equations (in potential form) and the 1D-3V particle orbit equations to produce a discrete system that remains exactly charge- and energy-conserving. Furthermore, enabled by the implicit Darwin equations, exact conservation of the canonical momentum per particle in any ignorable direction is enforced via a suitable scattering rule for the magnetic field. Several 1D numerical experiments demonstrate the accuracy and the conservation properties of the algorithm.

---

## 1. Introduction

The electromagnetic (EM) Particle-in-cell (PIC) method solves Vlasov-Maxwell's equations for kinetic plasma simulations [1, 2]. In the standard approach, Maxwell's equations are solved on a grid, and the Vlasov equation is solved by method of characteristics using a large number of particles, from which the evolution of the probability distribution function (PDF) is obtained. The field-PDF description is tightly coupled. Maxwell's equations (or a subset thereof) are driven by moments of the PDF such as charge density and/or current density. The PDF, on the other hand, follows a hyperbolic equation in phase space, whose characteristics are determined by the fields self-consistently.

To date, most PIC methods employ explicit time-stepping (e.g. leapfrog scheme), which can be very inefficient for long-time, large spatial scale simulations. The algorithmic inefficiency of standard explicit PIC is rooted in the presence of numerical stability constraints, which force both a minimum grid-size (due to the so-called finite-grid instability [1, 2], which requires resolution of the smallest Debye length) and a very small timestep (due to the well-known CFL constraint in the general electromagnetic case,  $c\Delta t < \Delta x$ , where  $c$  is speed of

---

\*Corresponding author

*Email address:* gchen@lanl.gov (G. Chen)

light, and  $\Delta t$  and  $\Delta x$  are the timestep and grid-size, respectively). Furthermore, numerical heating due to the lack of exact discrete energy conservation [1, 2] compromises the accuracy of explicit PIC simulations over long time scales, particularly for realistic ion-to-electron mass ratios. In the electromagnetic context, the accuracy issue is aggravated further by the presence of electromagnetic waves, which can be either unstable [3] or noisily excited to high levels [4].

Implicit methods, however, can free the PIC approach from numerical stability constraints, and thus have the potential of much improved algorithmic efficiency. This realization drove the exploration of implicit PIC starting in the 1980s [5–21]. These studies explored the viability of an implicit PIC formulation and its accuracy properties, and resulted in important developments such as the implicit-moment method [5–8, 13, 20] and the direct-implicit method [9, 11, 14, 17, 19]. However, limitations of the solver technology at the time forced early implicit PIC practitioners to rely on approximations such as linearization and lagging, which did not respect the strong field-particle coupling. These numerical approximations produced energy conservation errors that could result in significant plasma self-heating or self-cooling [22].

Fully implicit algorithms hold the promise of overcoming some of the difficulties of explicit and seim-implicit EM-PIC schemes. Some of these advantages were demonstrated in Ref. [23], where an energy-conserving fully implicit Vlasov-Maxwell EM-PIC scheme was proposed. However, it was shown in the reference that the approach suffered from radiative aliasing noise, which obscures physical signals as errors accumulate in time. The radiative noise disappeared by introducing some numerical damping in the discretization, but this in turn destroyed the exact energy conservation property.

In non-relativistic applications, radiative aliasing noise can be eliminated by ordering out light waves from Maxwell’s equations to arrive to the so-called Darwin model [24–27]. The Darwin field equations are no longer hyperbolic, but elliptic, rendering explicit time integration schemes unconditionally unstable [28]. Nielson and Lewis [28] introduced semi-implicit schemes to advance the Darwin-PIC system, which have become the standard for later development and applications of plasma Darwin-PIC simulations (see Refs. [21, 29–36] and references therein). Nevertheless, the resulting field equations, in either Hamiltonian or Lagrangian form, are complicated and difficult to solve, especially when non-periodic boundary conditions are employed [31, 32, 37, 38], and feature no exact conservation properties (e.g., local charge, total energy, or total momentum).

In contrast to earlier implicit Darwin-PIC studies, our focus here is on fully implicit, fully nonlinear PIC algorithms. We build upon recent developments in fully implicit electrostatic [39, 40] and electromagnetic [23] PIC algorithms, which enforce tight nonlinear convergence between particles and fields at every timestep. Their fully implicit character enables exact discrete conservation properties, such as energy and charge conservation, which are attractive for long-time simulations.

The purpose of this study is to demonstrate a fully implicit scheme for the Darwin model that conserves energy and charge exactly in a discrete setting, without suffering from enhanced radiative aliasing noise [23]. The Darwin equations are solved in potential form in a one-dimensional (1D) periodic system [25] using a Jacobian-free Newton-Krylov (JFNK) solver [23, 39]. Particle orbit equations involving three velocity components and one position are solved implicitly with particle sub-stepping and orbit-averaging [39, 41]. Special care

is taken when scattering the magnetic field to the particles, so that the particle canonical momentum in any ignorable direction is conserved exactly.

The aim and intent of this study resonates strongly with an earlier implementation of the 1D-3V Darwin-PIC model by Hasegawa et al. [25]. In this reference, the authors prove conservation theorems for local charge, global energy, and particle canonical momenta in a continuum-time Klimontovich representation of the plasma system. The study in the present paper goes beyond Hasegawa and co-author's in that the conservation theorems are proved in a discrete setting. The fully implicit character of our implementation turns out to be key to realize these discrete conservation properties.

The rest of the paper is organized as follows. Section 2 introduces our formulation for the general Vlasov-Darwin model and its favorable properties. The model is reduced to 1D-3V and discretized with an implicit particle-based central-difference scheme in Sec. 3, where we review our charge-conserving particle-moving strategy, and prove theorems for the exact conservation of global energy and particle canonical momenta in a discrete setting. Numerical examples demonstrating the properties of the algorithm are presented in Sec. 4. Finally, we conclude in Sec. 5.

## 2. Electromagnetic Vlasov-Darwin model

The general Vlasov-Darwin model for a collisionless electromagnetic plasma reads [27, 28, 38, 42, 43]:

$$\partial_t f_\alpha + \mathbf{v} \cdot \nabla f_\alpha + \frac{q_\alpha}{m_\alpha} (\mathbf{E} + \mathbf{v} \times \mathbf{B}) \cdot \nabla_v f_\alpha = 0, \quad (1)$$

$$\frac{1}{\mu_0} \nabla \times \nabla \times \mathbf{A} = -\frac{1}{\mu_0} \nabla^2 \mathbf{A} = \mathbf{j} - \epsilon_0 \partial_t \nabla \phi, \quad (2)$$

$$\epsilon_0 \nabla^2 \phi = -\rho, \quad (3)$$

$$\nabla \cdot \mathbf{A} = 0, \quad (4)$$

where  $f_\alpha(\mathbf{r}, \mathbf{v})$  is the particle distribution function of species  $\alpha$  in phase space,  $q_\alpha$  and  $m_\alpha$  are the species charge and mass respectively,  $\epsilon_0$  and  $\mu_0$  are the vacuum permittivity and permeability respectively,  $\phi$  and  $\mathbf{A}$  are the self-consistent electric and vector potential respectively. Unlike Maxwell's equations, the Darwin model does not feature Gauge invariance, and only the Coulomb gauge is physically acceptable (to enforce charge conservation [25, 27], as discussed below). The electric and magnetic fields are defined uniquely from  $\phi$ ,  $\mathbf{A}$  as:

$$\mathbf{E} = -\nabla \phi - \partial_t \mathbf{A} ; \mathbf{B} = \nabla \times \mathbf{A}. \quad (5)$$

The Darwin equations are driven by the plasma current density  $\mathbf{j} = \sum_\alpha q_\alpha \int f_\alpha \mathbf{v} d\mathbf{v}$  and charge density  $\rho = \sum_\alpha q_\alpha \int f_\alpha d\mathbf{v}$ .

The Vlasov-Darwin model in Eqs. 1-4 features two involutions, Poisson's equation and the solenoidal constraint of the vector potential. However, this system is overdetermined, and can be formulated much more succinctly, as we shall see. We begin by realizing that the local charge conservation equation,

$$\partial_t \rho + \nabla \cdot \mathbf{j} = 0, \quad (6)$$

can be derived independently from both the Vlasov equation (Eq. 1) and the Darwin electromagnetic model (Eqs. 2-4). From the Vlasov equation, Eq. 6 follows by taking its zeroth velocity moment for all species, and then adding them up according to the definition of the charge density. From the Darwin equations, the charge conservation equation follows by taking the divergence of Eq. 2, and using Eq. 3.

This redundancy in the model can be exploited to formulate a minimal set of Darwin equations such that, together with the Vlasov equation, the two involutions are implied in the formulation, and do not need to be enforced explicitly. This minimal Darwin model is comprised of two equations. The first equation is the vector Laplacian form of Eq. 2. The second equation is found by taking the divergence of Eq. 2 and using Eq. 4. Thus, our final set of Vlasov-Darwin equations reads:

$$\partial_t f_\alpha + \mathbf{v} \cdot \nabla f_\alpha + \frac{q_\alpha}{m_\alpha} (\mathbf{E} + \mathbf{v} \times \mathbf{B}) \cdot \nabla_v f_\alpha = 0, \quad (7)$$

$$-\frac{1}{\mu_0} \nabla^2 \mathbf{A} = \mathbf{j} - \epsilon_0 \partial_t \nabla \phi, \quad (8)$$

$$\epsilon_0 \partial_t \nabla^2 \phi = \nabla \cdot \mathbf{j}. \quad (9)$$

These three equations, together with the local charge conservation equation (which is implicit in Eq. 7), imply the involutions (Eqs. 3, 4). In particular, Poisson's equation (Eq. 3) is implied by Eq. 9 and the charge conservation equation. The solenoidal constraint is implied as well. This is seen by taking the divergence of Eq. 8 and using Eq. 9, to find:

$$\nabla^2 \nabla \cdot \mathbf{A} = 0,$$

from which, with appropriate boundary conditions, Eq. 4 follows. The boundary conditions must be consistent with  $\nabla \cdot \mathbf{A} = 0$  at the boundary [25] (i.e., must enforce continuity of the normal component of the vector potential at the boundary).

Equations 7, 8, and 9 constitute the minimal Vlasov-Darwin set of choice in this study. We emphasize that the main advantage of this set is that the two involutions (Poisson's equation and the solenoidal constraint of  $\mathbf{A}$ ) are implied, and thus do not need to be enforced or solved explicitly. This property, when implemented discretely, will be most advantageous, as ensuring (or avoiding) Eq. 4 has turned out to be one the most difficult implementation roadblocks of the Darwin approximation in multiple dimensions [28, 31]. This, however, will require a very careful discrete treatment, and in particular one that strictly conserves local charge.

### 3. One-dimensional implicit particle-based discretization of the Vlasov-Darwin model

In the remainder of this study, we specialize the Vlasov-Darwin equations to one spatial dimension and three velocity dimensions (1D-3V) in Cartesian geometry, as follows.<sup>1</sup> We

---

<sup>1</sup>We should point out that enforcing the solenoidal involution is trivial in this reduced dimensionality context, and therefore the point outlined in the previous section about implied involutions is not so critical for  $\nabla \cdot \mathbf{A} = 0$ . However, it will be key in multiple dimensions. We will comment on the extension of the current approach to multiple dimensions later in this paper.

consider a 1D periodic system, with  $\partial_y = \partial_z = 0$ , for which the Darwin model reduces to:

$$\epsilon_0 \partial_t E_x + j_x = \langle j_x \rangle, \quad (10)$$

$$\frac{1}{\mu_0} \partial_x^2 A_{y,z} + j_{y,z} = \langle j_{y,z} \rangle, \quad (11)$$

where  $E_x = -\partial\phi/\partial x$ , and the terms on the right hand side are the spatial average of the current densities, e.g.  $\langle j_x \rangle = \int j_x dx / \int dx$ . These are necessary in a periodic system to enforce periodicity of the fields [25, 39]. The inductive electric field is determined from the vector potential as:

$$E_{y,z} = -\partial_t A_{y,z}. \quad (12)$$

The magnetic field is determined from the vector potential as:

$$B_x = B_{0x}; \quad B_y = B_{0y} - \partial_x A_z; \quad B_z = B_{0z} + \partial_x A_y, \quad (13)$$

where  $(B_{0x}, B_{0y}, B_{0z})$  is a prescribed equilibrium magnetic field.

Discretizing the 1D equations with central difference in time gives for the electric field components:

$$\epsilon_0 \frac{E_{x,i+1/2}^{n+1} - E_{x,i+1/2}^n}{\Delta t} + j_{x,i+1/2}^{n+1/2} = \langle j_x \rangle, \quad (14)$$

$$E_{y,i}^{n+1/2} = -\frac{A_{y,i}^{n+1} - A_{y,i}^n}{\Delta t}, \quad (15)$$

$$E_{z,i}^{n+1/2} = -\frac{A_{z,i}^{n+1} - A_{z,i}^n}{\Delta t}, \quad (16)$$

where the superscript  $n$  denotes the time level at  $n\Delta t$ , the subscript  $i$  denotes the mesh point at  $i\Delta x$ , and  $\Delta t$  and  $\Delta x$  are time and spatial mesh intervals respectively for the field equations. The vector potential components are found from:

$$\frac{1}{\mu_0} \partial_x^2 \frac{A_y^{n+1} + A_y^n}{2} \Big|_i + j_{y,i}^{n+1/2} = \langle j_y \rangle, \quad (17)$$

$$\frac{1}{\mu_0} \partial_x^2 \frac{A_z^{n+1} + A_z^n}{2} \Big|_i + j_{z,i}^{n+1/2} = \langle j_z \rangle. \quad (18)$$

Note that the vector components along ignorable directions are defined at the integer spatial mesh points, while the  $x$ -components are defined at the half spatial mesh points. The  $\partial_x^2$  is discretized using a standard central-difference formula, e.g.  $\partial_x^2 A|_i = (A_{i+1} - 2A_i + A_{i-1})/\Delta x$ . Similarly, we obtain the magnetic field components as:

$$B_{y,i+1/2} = B_{0y} - \frac{A_{z,i+1} - A_{z,i}}{\Delta x}; \quad B_{z,i+1/2} = B_{0z} + \frac{A_{y,i+1} - A_{y,i}}{\Delta x}. \quad (19)$$

The current components are gathered from particles to ensure charge and energy conservation, as described later in this section.

Particle quantities are evolved from the 1D-3V particle equations of motion:

$$\partial_t x_p = v_{x,p}, \quad (20)$$

$$\partial_t v_{x,p} = \frac{q_p}{m_p} (E_{x,p} + v_{p,y} B_{z,p} - v_{p,z} B_{y,p}), \quad (21)$$

$$\partial_t v_{y,p} = \frac{q_p}{m_p} (E_{y,p} + v_{p,z} B_{x,p} - v_{p,x} B_{z,p}), \quad (22)$$

$$\partial_t v_{z,p} = \frac{q_p}{m_p} (E_{z,p} + v_{p,x} B_{y,p} - v_{p,y} B_{x,p}). \quad (23)$$

As in Ref. [39], these equations are discretized using a sub-stepped Crank-Nicolson scheme:

$$\frac{x_p^{\nu+1} - x_p^\nu}{\Delta\tau^\nu} = v_{x,p}^{\nu+1/2}, \quad (24)$$

$$\frac{v_{x,p}^{\nu+1} - v_{x,p}^\nu}{\Delta\tau^\nu} = \frac{q_p}{m_p} (E_{x,p}^{\nu+1/2} + v_{p,y}^{\nu+1/2} B_{z,p}^{\nu+1/2} - v_{p,z}^{\nu+1/2} B_{y,p}^{\nu+1/2}), \quad (25)$$

$$\frac{v_{y,p}^{\nu+1} - v_{y,p}^\nu}{\Delta\tau^\nu} = \frac{q_p}{m_p} (E_{y,p}^{\nu+1/2} + v_{p,z}^{\nu+1/2} B_{x,p}^{\nu+1/2} - v_{p,x}^{\nu+1/2} B_{z,p}^{\nu+1/2}), \quad (26)$$

$$\frac{v_{z,p}^{\nu+1} - v_{z,p}^\nu}{\Delta\tau^\nu} = \frac{q_p}{m_p} (E_{z,p}^{\nu+1/2} + v_{p,x}^{\nu+1/2} B_{y,p}^{\nu+1/2} - v_{p,y}^{\nu+1/2} B_{x,p}^{\nu+1/2}), \quad (27)$$

where the substep  $\Delta\tau^\nu$  satisfies  $\sum_{\nu=0}^{N_\nu} \Delta\tau^\nu = \Delta t$ , with  $\nu$  denoting the substep and  $N_\nu$  the number of substeps. Following earlier studies [44], the time step is determined here by a local error estimator  $\Delta\tau = 0.1 \min(\omega_t^{-1}, \omega_c^{-1})$ , where  $\omega_t = \frac{q}{m} |\partial_x E|$  is the electrostatic harmonic frequency, and  $\omega_c = \frac{q}{m} B$  is the gyrofrequency.

The scatter of the electric field to particles is defined as:

$$E_{x,p}^{\nu+1/2} = \sum_i \frac{E_{x,i+1/2}^{n+1} + E_{x,i+1/2}^n}{2} S_m(x_p^{\nu+1/2} - x_{i+1/2}), \quad (28)$$

$$E_{y,p}^{\nu+1/2} = - \sum_i \frac{A_{y,i}^{n+1} - A_{y,i}^n}{\Delta t} S_l(x_p^{\nu+1/2} - x_i), \quad (29)$$

$$E_{z,p}^{\nu+1/2} = - \sum_i \frac{A_{z,i}^{n+1} - A_{z,i}^n}{\Delta t} S_l(x_p^{\nu+1/2} - x_i), \quad (30)$$

where we have assumed that the electric field varies slowly during the timestep  $\Delta t$  [39]. Here,  $S_m$  is the B-spline of order  $m$ . We will be using  $m = 1$  and  $l = 2$  throughout this study. The latter ensures a linear interpolation of the magnetic field to the particles. The scattering of the magnetic field components to the particles will be determined such that the particle canonical momentum in both  $y$  and  $z$  directions is conserved exactly, and will be discussed later in this paper.

The current components needed in Eqs. 14, 17, and 18 are found from particle quantities as:

$$\bar{j}_{x,i+1/2}^{n+1/2} = \frac{1}{\Delta t \Delta x} \sum_p \sum_\nu q_p v_{p,x}^{\nu+1/2} S_m(x_p^{\nu+1/2} - x_{i+1/2}) \Delta\tau^\nu, \quad (31)$$

$$\bar{J}_{y,i}^{n+1/2} = \frac{1}{\Delta t \Delta x} \sum_p \sum_\nu q_p v_{p,y}^{\nu+1/2} S_l(x_p^{\nu+1/2} - x_i) \Delta \tau^\nu, \quad (32)$$

$$\bar{J}_{z,i}^{n+1/2} = \frac{1}{\Delta t \Delta x} \sum_p \sum_\nu q_p v_{p,z}^{\nu+1/2} S_l(x_p^{\nu+1/2} - x_i) \Delta \tau^\nu, \quad (33)$$

where we have added an overbar to denote that the current components are orbit averaged. Note that  $\bar{J}_{y,i}^{n+1/2}$  and  $\bar{J}_{z,i}^{n+1/2}$  use a spline order different from  $\bar{J}_{x,i+1/2}^{n+1/2}$  for consistency with those used by the electric field components (which will in turn be required for exact energy conservation). Next, we comment on our procedure to ensure exact charge conservation, and derive energy and canonical momenta conservation theorems.

### 3.1. Charge conservation

Exact local charge conservation can be ensured kinematically by pushing particles following the prescription outlined in Ref. [39]. In particular, for  $m \leq 1$ , the continuity equation is satisfied to numerical round-off whenever particles are forced to land at cell boundaries along their orbit.

We should note that the use of different spline orders in the current components in Eqs. 31-33 does not break charge conservation, because the current components in the ignorable directions do not enter the 1D continuity equation. We should also note that this prescription can be generalized to multiple dimensions [44].

### 3.2. Energy conservation theorem

As in earlier studies [25, 39, 44, 45], we begin by dotting the particle velocity equations, Eqs. 21-23, with the averaged velocity  $\mathbf{v}^{\nu+1/2}$ , orbit averaging all substeps, and summing over all particles, to find:

$$\begin{aligned} \frac{K^{n+1} - K^n}{\Delta t} &= \sum_p \frac{1}{\Delta t} \sum_\nu m_p \frac{\mathbf{v}_p^{\nu+1} + \mathbf{v}_p^\nu}{2} \cdot \frac{\mathbf{v}_p^{\nu+1} - \mathbf{v}_p^\nu}{\Delta \tau^\nu} \Delta \tau^\nu = \sum_p \frac{1}{\Delta t} \sum_\nu q_p (\mathbf{v}_p \cdot \mathbf{E}_p)^{\nu+1/2} \Delta \tau^\nu \\ &= \sum_i \Delta x \left( E_{x,i+1/2}^{n+1/2} \bar{J}_{x,i+1/2}^{n+1/2} + E_{y,i}^{n+1/2} \bar{J}_{y,i}^{n+1/2} + E_{z,i}^{n+1/2} \bar{J}_{z,i}^{n+1/2} \right), \end{aligned}$$

where  $K \equiv \sum_p \frac{1}{2} m_p v_p^2$  is the total particle kinetic energy, and we have used Eqs. 28-30 and 31-33, assuming that the cell width  $\Delta x$  is uniform across the domain. Plugging in Eqs. 14-18, we find:

$$\begin{aligned} \sum_i \Delta x E_{x,i+1/2}^{n+1/2} \bar{J}_{x,i+1/2}^{n+1/2} &= -\epsilon_0 \sum_i \Delta x \frac{E_{x,i+1/2}^{n+1} + E_{x,i+1/2}^n}{2} \frac{E_{x,i+1/2}^{n+1} - E_{x,i+1/2}^n}{\Delta t} \\ &= -\frac{\epsilon_0}{2\Delta t} \sum_i \Delta x \left[ \left( E_{x,i+1/2}^{n+1} \right)^2 - \left( E_{x,i+1/2}^n \right)^2 \right] = -\frac{W_{\phi x}^{n+1} - W_{\phi x}^n}{\Delta t}, \\ \sum_i \Delta x E_{y,i}^{n+1/2} \bar{J}_{y,i}^{n+1/2} &= \frac{1}{\mu_0} \sum_i \Delta x \left( \frac{A_{y,i}^{n+1} - A_{y,i}^n}{\Delta t} \right) \left( \partial_x^2 \frac{A_y^{n+1} + A_y^n}{2} \right)_i \\ &= -\frac{1}{2\mu_0 \Delta t} \sum_i \Delta x \left[ \left( \partial_x A_y^{n+1} \right)_{i+1/2}^2 - \left( \partial_x A_y^n \right)_{i+1/2}^2 \right] = -\frac{W_{Bz}^{n+1} - W_{Bz}^n}{\Delta t}, \\ \sum_i \Delta x E_{z,i}^{n+1/2} \bar{J}_{z,i}^{n+1/2} &= -\frac{1}{2\mu_0 \Delta t} \sum_i \Delta x \left[ \left( \partial_x A_z^{n+1} \right)_{i+1/2}^2 - \left( \partial_x A_z^n \right)_{i+1/2}^2 \right] = -\frac{W_{By}^{n+1} - W_{By}^n}{\Delta t}. \end{aligned}$$

In these equations,  $W_{\phi x} \equiv \frac{\epsilon_0}{2} \sum_i \Delta x E_{x,i+1/2}^2$  is the electrostatic energy, and  $W_{By,z} \equiv \frac{1}{2\mu_0} \sum_i \Delta x (B_{y,z} - B_{0y,z})^2$  is the magnetic energy. Numerical spatial derivatives have been telescoped, as allowed by a standard central finite differencing of the spatial second-order derivative. The terms associated with the average currents in Eqs. 14, 17 and 18 cancel exactly because  $\sum_i E_{x,i+1/2} = 0$  and  $\sum_i E_{y,i} = \sum_i E_{z,i} = 0$ . The former follows from  $E_x$  being a gradient in a periodic domain. The latter follow because the average of the corresponding vector potential component satisfying Eqs. 17, 18 in a periodic domain is conserved in time (see App. Appendix A). This property transfers to the discrete when the standard discretization of  $\partial_x^2 A_{y,z}$  is used. As a result,  $\sum_i A_{y,i}^{n+1} = \sum_i A_{y,i}^n$  and similarly with  $A_z$ . The energy conservation theorem sought follows:

$$(K_p + W_{\phi x} + W_{By} + W_{Bz})^{n+1} = (K_p + W_{\phi x} + W_{By} + W_{Bz})^n. \quad (34)$$

### 3.3. Conservation of particle canonical momenta

One subtlety of the one dimensional electromagnetic system is that the  $y$  and  $z$  components of the particle canonical momentum  $\mathbf{p} = m\mathbf{v} + q\mathbf{A}$  should be conserved, for each particle, for all time. This is a consequence of the system Lagrangian  $\mathcal{L} = m\mathbf{v}^2/2 + q(\mathbf{v} \cdot \mathbf{A} - \phi)$  being independent of the  $y$  and  $z$  coordinates, as can be shown from the Euler-Lagrange equations:

$$\frac{d}{dt} \left( \frac{\partial \mathcal{L}}{\partial v_q} \right) = \frac{\partial \mathcal{L}}{\partial q}.$$

The canonical momentum is defined as  $\mathbf{p} = \frac{\partial \mathcal{L}}{\partial \mathbf{v}}$ , and hence is clear that for  $q = y, z$ :

$$\dot{p}_y = \dot{p}_z = 0. \quad (35)$$

We seek to enforce this conservation property exactly. As we shall see, this will constrain the form of the scattering of the magnetic field to the particles in Eqs. 21-23. Let's focus on the conservation of  $p_y$ :

$$\dot{p}_y = m_p \dot{v}_{p,y} + q_p \dot{A}_{y,p} = 0, \quad (36)$$

where

$$A_{y,p} \equiv \sum_i A_{y,i} S_l(x_p - x_i). \quad (37)$$

Equation 36 can be integrated over a substep  $\nu$  to  $\nu + 1$ , to find (ignoring the subscript  $y$ ):

$$(m_p v_p + q_p A_p)^{\nu+1} - (m_p v_p + q_p A_p)^\nu = 0, \quad (38)$$

which can be rearranged as :

$$\frac{v_p^{\nu+1} - v_p^\nu}{\Delta \tau^\nu} = -\frac{q_p}{m_p} \sum_i \frac{A_i^{\nu+1} S_l(x_p^{\nu+1} - x_i) - A_i^\nu S_l(x_p^\nu - x_i)}{\Delta \tau^\nu} \quad (39)$$

Specializing this result for second-order splines ( $l = 2$ ), Taylor-expanding the shape function, and casting Eq. 39 into the form of Eq. 26 gives (see App. Appendix B),

$$B_{z,p}^{\nu+1/2} = B_{0,z} + \sum_i \left[ \frac{A_{y,i+1}^{\nu+1/2} - A_{y,i}^{\nu+1/2}}{\Delta x} S_1(x_{i+1/2} - x_p^{\nu+1/2}) \right] + \frac{\Delta A_{y,i_p-1}^{\nu+1/2} - 2\Delta A_{y,i_p}^{\nu+1/2} + \Delta A_{y,i_p+1}^{\nu+1/2}}{8\Delta x^2} (x_p^{\nu+1} - x_p^\nu). \quad (40)$$

The first term on the right hand side is the central-difference approximation of  $B_z = \partial_x A_y$  at the particle location. In the second term,  $\Delta A_{y,i_p}^{\nu+1/2} = A_{i_p}^{\nu+1} - A_{i_p}^{\nu}$ . The second term is an  $O(\Delta\tau^2)$  correction (commensurate with the truncation error of the Crank-Nicolson scheme) evaluated at the particle cell index  $i_p$  that ensures exact conservation of the particle canonical momentum. A similar procedure for the conservation of  $p_z$  yields:

$$B_{y,p}^{\nu+1/2} = B_{0,y} - \sum_i \left[ \frac{A_{z,i+1}^{\nu+1/2} - A_{z,i}^{\nu+1/2}}{\Delta x} S_1(x_{i+1/2} - x_p^{\nu+1/2}) \right] - \frac{\Delta A_{z,i_p-1}^{\nu+1/2} - 2\Delta A_{z,i_p}^{\nu+1/2} + \Delta A_{z,i_p+1}^{\nu+1/2}}{8\Delta x^2} (x_p^{\nu+1} - x_p^{\nu}). \quad (41)$$

Note that, in 1D,  $B_x$  must remain constant in space (because  $\nabla \cdot \mathbf{B} = \partial B_x / \partial x = 0$ ) and time (because  $\partial_t B_x = \partial E_z(x) / \partial y - \partial E_y(x) / \partial z = 0$ ). The proposed scattering formula for the magnetic field components along ignorable directions guarantees conservation of canonical momentum for every particle sub-step. Conservation over the macro-step follows straightforwardly by integration over all substeps.

### 3.4. Binomial smoothing

As in earlier studies [1, 39], we apply binomial smoothing to reduce noise level of high  $k$  modes introduced by particle-grid interpolations [1]. Smoothing preserves the conservation properties of the implicit Darwin model when implemented appropriately. The governing Darwin-PIC equations with binomial smoothing read:

$$\epsilon_0 \frac{E_{x,i+1/2}^{n+1} - E_{x,i+1/2}^n}{\Delta t} + SM(j_x^{n+1/2})_{i+1/2} - \langle j_x \rangle = 0, \quad (42)$$

$$\frac{1}{\mu_0} \partial_x^2 \frac{A_y^{n+1} + A_y^n}{2} \Big|_i + SM(j_y^{n+1/2})_i - \langle j_y \rangle = 0, \quad (43)$$

$$\frac{1}{\mu_0} \partial_x^2 \frac{A_z^{n+1} + A_z^n}{2} \Big|_i + SM(j_z^{n+1/2})_i - \langle j_z \rangle = 0. \quad (44)$$

$$\frac{x_p^{\nu+1} - x_p^{\nu}}{\Delta t} - v_{x,p}^{\nu+1/2} = 0, \quad (45)$$

$$\frac{\mathbf{v}_p^{\nu+1} - \mathbf{v}_p^{\nu}}{\Delta t} - \frac{q_p}{m_p} \left( SM(\mathbf{E}^{n+1/2})_p + \mathbf{v}_p^{\nu+1/2} \times SM(\mathbf{B}^{\nu+1/2})_p \right) = 0, \quad (46)$$

with the binomial operators  $SM_i$  and  $SM_p$  defined as:

$$SM(Q)_i = \frac{Q_{i-1} + 2Q_i + Q_{i+1}}{4}, \quad (47)$$

and

$$SM(Q)_p = \sum_i SM(Q)_i S(x_p - x_i). \quad (48)$$

Owing to the property in periodic domains that  $\sum_i A_i SM(B)_i = \sum_i B_i SM(A)_i$ , it is straightforward to show that energy and charge conservation theorems remain valid [39]. Canonical momenta conservation also survives when replacing  $A$  by  $SM(A)$  in the last section, giving:

$$SM(B_z^{\nu+1/2})_p = \sum_i \left[ \frac{SM(A_y^{\nu+1/2})_{i+1} - SM(A_y^{\nu+1/2})_i}{\Delta x} S_1(x_{i+1/2} - x_p^{\nu+1/2}) \right] +$$

$$+ \frac{SM(\Delta A_y^{\nu+1/2})_{i_p-1} - SM(2\Delta A_y^{\nu+1/2})_{i_p} + SM(\Delta A_y^{\nu+1/2})_{i_p+1}}{8\Delta x^2} (x_p^{\nu+1} - x_p^\nu).$$

i.e.,  $B_z$  must be scattered to particles from the binomially smoothed  $A_y$ . A similar result is found for  $SM(B_y^{\nu+1/2})_p$ .

#### 4. Numerical tests

The set of field equations (42-44) and particle equations (45-46) are the ones solved in this study. For this, we employ a JFNK nonlinear solver, implemented and configured as described in Ref. [39]. As in the reference, the particle equations are enslaved to the field equations (particle enslavement), which requires only a single copy of the particle population. This results in minimal memory requirements for the nonlinear solver, determined only by the storage required by the field quantities.

In this section, we provide a sequence of numerical tests of increasing complexity to provide verification against linear theory results (measured as instability growth rates), and to demonstrate the favorable properties of the approach. These tests are (from simplest to more complex): an electron Weibel instability, an ion Weibel instability, and a kinetic Alfvén wave problem. The first two tests are for non-magnetized plasmas, and the last one is for a magnetized plasma. The last two tests are stiff multiscale problems due to the ion-to-electron mass disparity (all numerical tests employ a realistic mass ratio  $m_i/m_e = 1836$ ).

For these numerical tests, we normalize the Darwin PIC equations with appropriate reference quantities:

$$\begin{aligned} \hat{t} &= t\omega_0, & \hat{x} &= \frac{x}{x_0}, & \hat{v} &= \frac{v}{v_0}, \\ \hat{n} &= \frac{n}{n_0}, & \hat{q} &= \frac{q}{q_0}, & \hat{m} &= \frac{m}{m_0}, \\ \hat{E} &= \frac{\varepsilon_0 E}{q_0 n_0 x_0}, & \hat{A} &= \frac{A}{\mu_0 q_0 n_0 x_0^3}, & \hat{J} &= \frac{J}{q_0 n_0 x_0 \omega_0}, \end{aligned} \quad (49)$$

to find:

$$\frac{\partial \hat{E}_x}{\partial \hat{t}} + \hat{J}_x = \langle \hat{J}_x \rangle, \quad (50)$$

$$\partial_x^2 \hat{A}_{y,z} + \hat{j}_{y,z} = \langle \hat{j}_{y,z} \rangle, \quad (51)$$

$$\hat{E}_{y,z} = -\frac{\partial \hat{A}_{y,z}}{\partial \hat{t}}, \quad (52)$$

$$\hat{B}_{y,z} = (\nabla \times \hat{\mathbf{A}})_{y,z} \quad (53)$$

$$\frac{d\hat{x}_p}{d\hat{t}} = \hat{v}_p, \quad (54)$$

$$\frac{d\hat{v}_p}{d\hat{t}} = \hat{a}_p, \quad (55)$$

where  $\hat{a}_p = \frac{q_p}{m} [\hat{E}_p + \hat{v}_p \times \hat{B}_p]$ . In a two-species system, we pick either electrons or ions as the reference species, depending on the problem of interest. For electrons, the associated

reference constants are:

$$\begin{aligned}
v_0 &= c \\
x_0 &= d_e (= c/\omega_{pe}), \\
\omega_0 &= \omega_{pe}, \\
n_0 &= \frac{W_e}{d_e}, \\
q_0 &= \frac{n_e d_e e}{W_e}, \\
m_0 &= \frac{n_e d_e m_e}{W_e},
\end{aligned} \tag{56}$$

where  $W_e = N_e/\hat{N}_e$  is the ratio of the number of real particles and simulated particles. Similar reference values are found for ions. Note that, in our units, the magnetic field reference value is measured in units of  $\hat{B} = \omega_{cs}/\omega_{ps}$ , for  $s = e$  or  $i$ .

#### 4.1. The electron Weibel instability

The Weibel instability is an electromagnetic instability that can appear in a unmagnetized plasma due to velocity-space anisotropy [46, 47]. In a Cartesian coordinate system, a perturbation of the magnetic field perpendicular to the wave vector  $\mathbf{k}$  (which is along the  $x$  direction) can induce a plasma current that increases the perturbation, provided that the plasma is hotter in the perpendicular direction (i.e.  $y$  and  $z$ ). By making either the electron or ion velocity distribution anisotropic, we can have the electron or ion Weibel instability, respectively.

For the electron Weibel instability, we choose electrons as the reference species. For the initialization of the particle distribution, we introduce particles in pairs to obtain zero plasma current exactly for each species. The two particles of each pair are set at the same location with opposite velocities. The initial distribution function is

$$f(x, v, t = 0) = f_M(v) [1 + a \cos(k_x x)] \tag{57}$$

where  $f_M$  is the Maxwellian distribution,  $a$  is the perturbation level,  $k_x$  is the perturbed wave number. The spatial distribution is approximated by first putting ions randomly with a constant distribution, e.g.  $x_0 \in [0, L]$ . The electrons are distributed in pairs with ions according to the Debye distribution [48]. Specifically, in each  $e$ - $i$  pair, the electron is situated away from the ion by a small distance,  $dx = \ln(R)$  where  $R \in (0, 1)$  is a uniform random number. The perturbation is done by shifting the particle position by a small amount such that  $x = x_0 + a \cos(k_x x_0)$ , where  $x_0$  is the initial particle position,  $a = 0.01$ , and  $k_x = \frac{2\pi}{L}$  with  $L$  the domain size.

The plasma consists of electrons and singly charged ions, with a realistic mass ratio  $m_i/m_e = 1836$ . The simulated domain is of  $\pi$  in length, with 64 uniform cells and periodic boundary conditions. The average number of particles per cell of each species is 2000. Electrons are initialized with an anisotropic Maxwell distribution with  $T_{ey,z}/T_{ex} = 16$ , and the thermal velocity parallel to the wave vector is  $v_{eTx} \equiv \sqrt{T_{ex}/m} = 0.1$ . Ions are initialized with an isotropic Maxwell distribution with  $v_{iT_x} = 0.1$ . The timestep is taken to be  $\Delta t = 1$ .

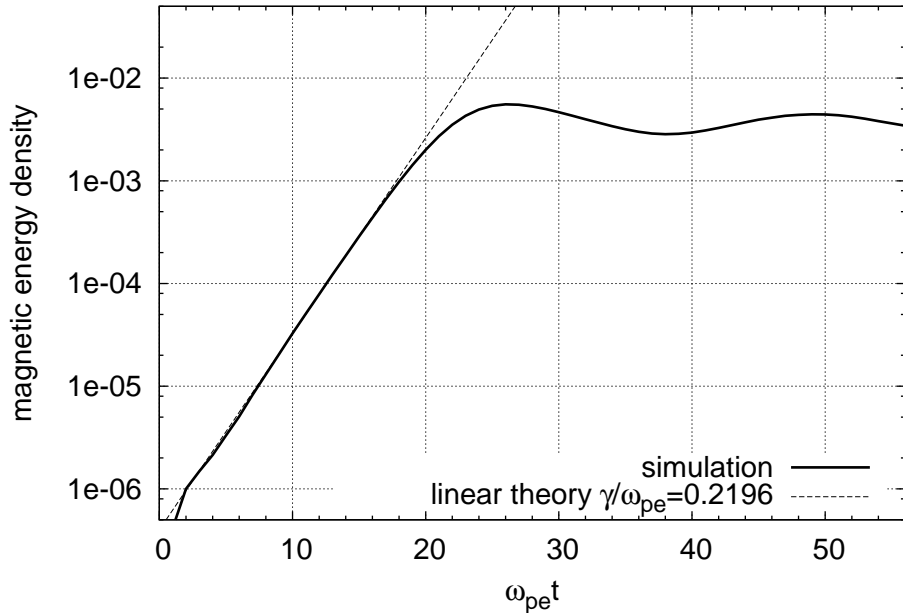


Figure 1: Time history of the magnetic field energy  $W_A = \sum_i (B_{y,i+1/2}^2 + B_{z,i+1/2}^2)/2$  evolving from an electron Weibel instability. Excellent agreement with the theoretical linear growth rate is found.

For comparison, the linear growth rate ( $\gamma = 0.22$ ) is found from the dispersion relation of electromagnetic waves in a bi-Maxwellian plasma [49]:

$$1 - \frac{k_x^2 c^2}{\omega^2} - \sum_{\alpha} \frac{\omega_{p\alpha}^2}{\omega^2} \left( 1 + \frac{T_{\alpha y,z}}{2T_{\alpha x}} Z'(\xi_{\alpha}) \right) = 0, \quad (58)$$

where  $\alpha = e, i$ ,  $\xi_{\alpha} = \omega/k_x \sqrt{2T_{\alpha x}/m_{\alpha}}$ , and  $Z'(\xi)$  is the first derivative of plasma dispersion function. The agreement between the simulation and theory is shown in Fig. 1. The time history of conserved quantities (e.g., charge, energy, momentum, and canonical momenta) of the simulated system is depicted in Fig. 2. We see that charge conservation is at the computer round-off level. Energy conservation is determined by the JFNK nonlinear tolerance level (a relative tolerance of  $10^{-8}$  is used in this study), and the canonical momenta conservation is determined by the Picard tolerance level for orbit integration (a relative tolerance of  $10^{-10}$  is used). As in earlier studies [39], the particle momentum in the  $x$  direction is not conserved exactly, but the error is relatively small.

#### 4.2. The ion Weibel instability

Next, we simulate the ion Weibel instability, which is more challenging because electron dynamics makes the problem very stiff. We keep the same mass ratio  $m_i/m_e = 1836$ , but use ions as the reference species for normalization. The simulated domain is of  $\frac{2\pi}{3} \sqrt{m_e/m_i}$  in length, with 64 uniformly distributed cells (corresponding to a cell width about 30 times larger than the Debye length), periodic boundary conditions, and 2000 particles per cell of each species. The electron species is initialized with an isotropic Maxwell distribution. We

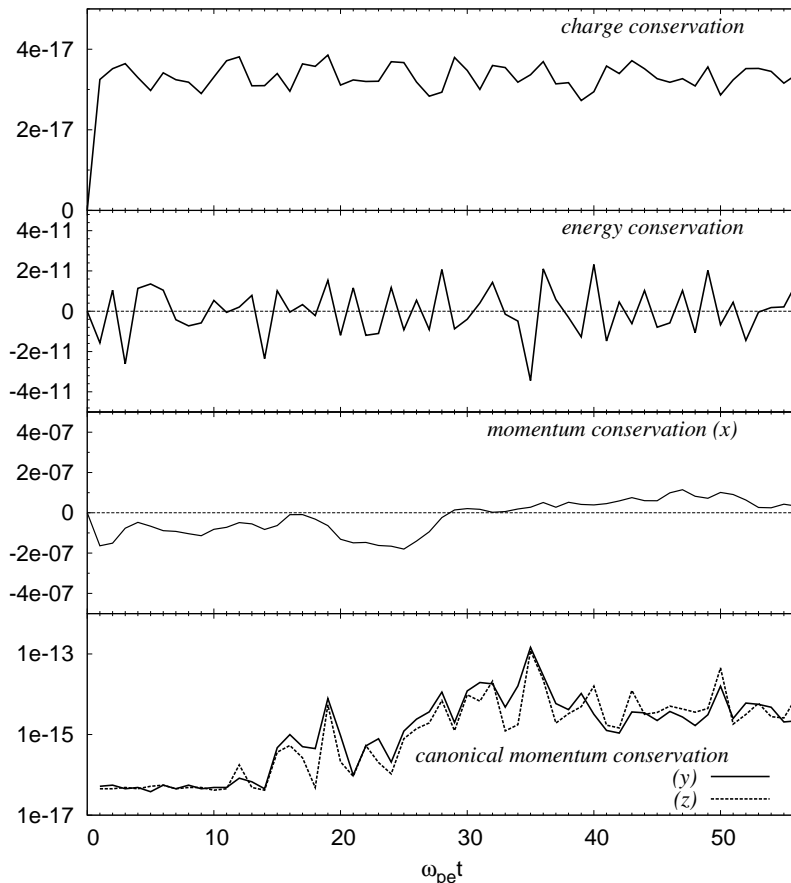


Figure 2: Conserved quantities in the simulation of the electron Weibel instability. Charge conservation is measured as the (root-mean-square) rms of the continuity equation, numerically evaluated at grid cells  $\sqrt{\sum_i (\rho_i^{n+1} - \rho_i^n + \Delta t(\bar{j}_{i+1/2} - \bar{j}_{i-1/2})/\Delta x)^2/N_g}$  where  $N_g$  is the number of grid-points. Energy conservation is measured as the change in the total energy (c.f. Eq. 34) between successive time steps. Momentum conservation in the  $x$  direction is measured as  $\sum_p m_p v_{p,x} / \sum_\alpha m v_{th,x}$ , where  $p$  and  $\alpha$  indicate particle and species index respectively. Finally, the maximum error in the conservation of canonical momenta for all particles is measured as  $\max_p (|m_p v_p^{n+1} + q_p A_p^{n+1} - m_p v_p^n - q_p A_p^n|)$  in the  $y$  and  $z$  directions, respectively.

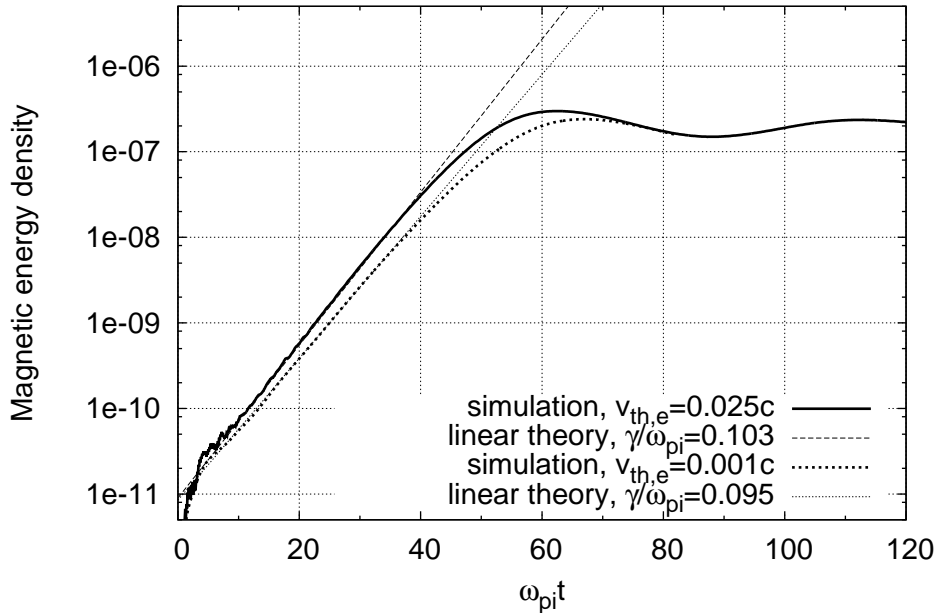


Figure 3: Time history of the magnetic field energy  $W_A = \sum_i (B_{y,i+1/2}^2 + B_{z,i+1/2}^2)/2$  from the ion Weibel instability. Excellent agreement with the theoretical growth rates for different electron thermal velocities is found.

consider two electron thermal velocities,  $v_{eTx} = 0.001$  and  $v_{eTx} = 0.025$ . The ion species is initialized with an anisotropic Maxwellian with  $T_{iy,z}/T_{ix} = 40,000$  and  $v_{iT_x} = 0.001$ . The timestep is taken to be  $\Delta t = 0.1\omega_{pi}^{-1}$ , which is about a factor of 40 times larger than the Vlasov-Maxwell-PIC CFL. Relatively large growth rates occur at large  $k_x$  and large energy anisotropies, consistent with those observed in Ref. [50] (in which the anisotropy is introduced by a cross-field ion flow). Figure 3 shows the time history of the magnetic field energy density for the two electron thermal velocities. Linear theory predicts growth rates of  $9.5 \times 10^{-2}$  and  $2.5 \times 10^{-2}$  for  $v_{eTx} = 0.001$  and  $0.025$ , respectively, which are in excellent agreement with simulations.

#### 4.3. The kinetic Alfvén wave ion-ion streaming instability

Finally, we consider the excitation of kinetic Alfvén waves by ion-ion streaming [51]. The instability is caused by interactions between the wave and the streaming ions. The simulation parameters are chosen to be similar to those presented in Ref. [51]. The mass ratio is  $m_i/m_e = 1836$ . We use ions as the reference species. The simulated domain is  $\frac{4\pi}{3}$  in length, with 64 uniformly distributed cells (with each cell about 40 times larger than the Debye length) and periodic boundary conditions, and the average number of particles per cell of one species is 2000. The external magnetic field  $B_0 = 0.00778$  is set to be at a large angle  $\theta = 70^\circ$  with respect to the propagation direction ( $x$ ) of the wave. The plasma consists of Maxwellian electrons with  $v_{eT} = 0.0745$  ( $\beta_e = 0.1$ ), and two singly charged ion components, i.e., an ambient ion component  $a$  and an ion beam component  $b$ , with number densities  $n_a = 0.6n_e$  and  $n_b = 0.4n_e$  (where  $n_e$  is the electron density). The two ion components have  $v_{aT} = 0.0192$  and  $v_{bT} = 0.0745$ , and a relative streaming speed with respect to each other

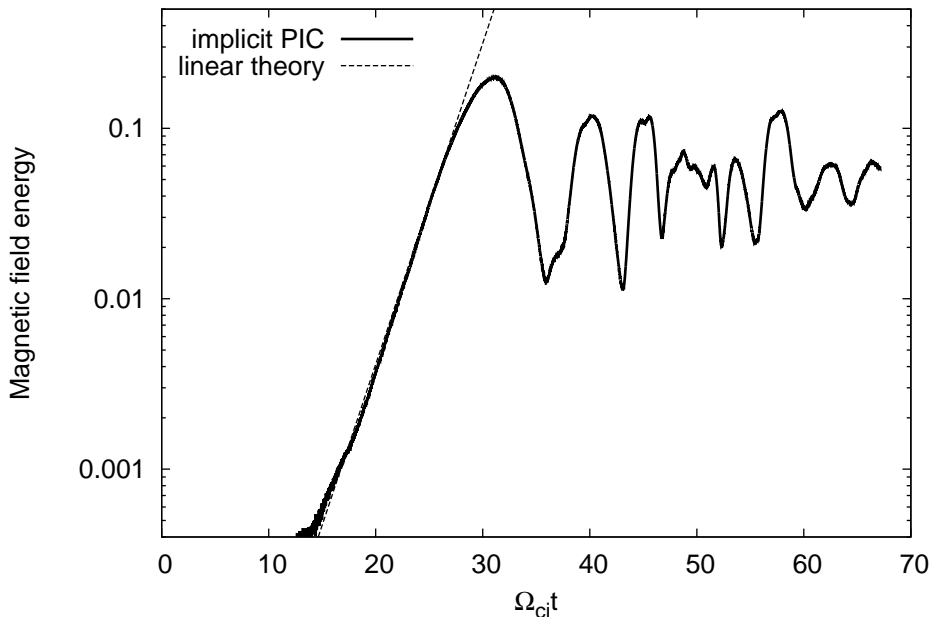


Figure 4: Time history of the magnetic field energy of the kinetic Alfvén wave ion-ion streaming instability simulation, demonstrating excellent agreement with linear theory.

of  $v_d = 2.5v_A$ , with  $v_A = \sqrt{m_e/m_i}/3$  the Alfvén speed along the external magnetic field direction. The timestep is again set to  $\Delta t = 0.1\omega_{pi}^{-1}$  (about 20 times larger than the explicit CFL). Figure 4 shows the simulation result of the magnetic energy density, which is again in excellent agreement with linear theory (the growth rate for this configuration is reported in Ref. [51] to be  $\gamma = 0.218\omega_{pi}/\omega_{ci}$ ).

## 5. Discussion and conclusions

This study introduces a fully implicit Darwin-PIC algorithm that employs a time-space-centered finite difference scheme for the coupled Darwin field and particle equations. The non-radiative limit of Maxwell’s equations is of interest in non-relativistic regimes to avoid radiative aliasing noise and/or instabilities [3, 4], particularly in the context of exactly energy conserving schemes [23]. We have used a potential formulation of the Darwin field equations, in terms of vector potential  $\mathbf{A}$  and electrostatic potential  $\phi$  (or equivalently  $E_x$  in the 1D case), and standard Lagrangian particle equations of motion (expressed in terms of position  $\mathbf{x}$  and velocity  $\mathbf{v}$ ). The stability of the algorithm is guaranteed by the fully implicit nature of the scheme. In contrast to previous Darwin-PIC algorithms [1, 28], the algorithm conserves global energy and local charge exactly in the discrete. It also conserves particle canonical momenta in the ignorable directions exactly, by carefully prescribing the magnetic field scattering formula. A necessary condition for the energy conservation is the exact reversibility of the time difference scheme, which is guaranteed by our time-centered implicit discretization. Just as in the electrostatic case [39], charge conservation is achieved by forcing particles to stop at cell boundaries as they traverse their orbits, and by using first-order splines to

gather the current density. Orbit-averaging and binomial smoothing are introduced without breaking the conservation properties of the scheme. Challenging, stiff multiscale numerical tests have demonstrated the advertised properties of the scheme, and its ability to employ large time steps and cell sizes stably.

As in the electrostatic case [52], the ability of the fully implicit Darwin-PIC approach to use large time steps and cell sizes indicates much potential for algorithmic acceleration vs. explicit Maxwell-PIC schemes (explicit Darwin-PIC implementations are not available for such a comparison). Since the CFL condition of explicit EM-PIC schemes (determined by the light speed) is more stringent than that of explicit ES-PIC (determined by the fastest thermal speed), we expect larger CPU speedups for implicit Darwin-PIC than ES-PIC for comparable simulation parameters. We also expect the convergence properties of the nonlinear solver to play a critical role in the overall efficiency of the implicit Darwin-PIC algorithm. Both of these are confirmed by the following back-of-the-envelope analysis, which closely follows that in Ref. [39] for ES-PIC (recently confirmed numerically in Ref. [52]).

We begin by estimating the CPU cost for a given PIC solver to advance the solution for a given time span  $\Delta T$  as [39]:

$$CPU = \frac{\Delta T}{\Delta t} N_{pc} \left( \frac{L}{\Delta x} \right)^d C, \quad (59)$$

where  $N_{pc}$  is the number of particles per cell,  $(L/\Delta x)$  is the number of cells per dimension,  $d$  is the number of physical dimensions, and  $C$  is the computational complexity of the solver employed, measured in units of a standard explicit PIC Vlasov-Maxwell leap-frog timestep. Accordingly, the implicit-to-explicit speedup is given by:

$$\frac{CPU_{ex}}{CPU_{im}} \sim \left( \frac{\Delta x_{im}}{\Delta x_{ex}} \right)^d \left( \frac{\Delta t}{\Delta t_{ex}} \right) \frac{C_{ex}}{C_{im}},$$

where we have assumed the same  $N_{pc}$  for both explicit and implicit schemes, and we denote  $\Delta t$  to be the implicit timestep. For simplicity, we assume that all particles take a fixed sub-timestep  $\Delta\tau$  in the implicit scheme, and that the cost of one time step with the explicit PIC solver is comparable to that of a single implicit sub-step. It follows that  $C_{im}/C_{ex} \sim N_{FE} (\Delta t/\Delta\tau_{im})$ , i.e., the cost of the implicit solver exceeds that of the explicit solver by the number of function evaluations ( $N_{FE}$ , which is a measure of the number of orbit evaluations) per  $\Delta t$  multiplied by the number of particle sub-steps ( $\Delta t/\Delta\tau_{im}$ , a measure of the cost per orbit). As in earlier studies [39, 52], we consider an implicit time step comparable to ion time scales, i.e.  $\Delta t \sim \omega_{pi}^{-1}$ . Assuming typical values for  $\Delta\tau_{im} \sim \min[0.1\Delta x_{im}/v_{th}, \omega_{ce}^{-1}, \omega_{pi}^{-1}]$ ,  $\Delta t_{ex} \sim \Delta x_{ex}/c$ ,  $\Delta x_{ex} \sim \lambda_D$ ,  $\Delta t \sim \omega_{pi}^{-1}$  and  $\Delta x_{im} \sim 0.2/k$ , we find that the CPU speedup scales as:

$$\frac{CPU_{ex}}{CPU_{imp}} \sim \frac{0.2}{(5k\lambda_D)^d} \frac{c}{v_{th,e}} \min \left[ \frac{1}{k\lambda_D}, \frac{c}{v_A} \sqrt{\frac{m_i}{m_e}}, \sqrt{\frac{m_i}{m_e}} \right] \frac{1}{N_{FE}}, \quad (60)$$

where  $v_A = B_0/\sqrt{n_e m_i \mu_0}$  is the Alfvén speed. Compared with the ES case [52], the EM CPU speedup is larger by a factor of  $c/v_{th,e}$ , as expected. As in the ES case, Eq. 60 confirms that the CPU speedup is inversely proportional to  $N_{FE}$ . This motivates future work towards the development of suitable fluid preconditioning strategies, as was done in Ref. [52] for the electrostatic case.

Finally, we acknowledge that the extension of the 1D-3V implicit Darwin-PIC formulation to multiple dimensions is not straightforward, particularly given the challenges documented in the literature [28, 31]. A main roadblock described in these studies is related to the enforcement of the solenoidal constraint of the vector potential (or rather, the complications stemming from its avoidance, particularly in regards to boundary condition specification for the transverse component of the electric field). In this regard, the Vlasov-Darwin formulation considered in Sec. 2 gives us reason for optimism, since both the solenoidal constraint and Poisson's equation are implicitly enforced in the continuum, and the transverse component of the electric field can be readily found from the vector potential. In the discrete, a necessary condition for the tractability of this formulation is the ability to enforce exact local charge conservation in multiple dimensions, which is within our reach [39, 44]. The implementation and demonstration of a multidimensional version of our implicit Darwin-PIC algorithm will be the subject of future work.

## Appendix A. Time-preservation of the spatial average of a field satisfying Poisson's equation in a 1D periodic domain

We demonstrate that a field  $\xi(x, t)$  satisfying Poisson's equation,

$$\nabla^2 \xi = S(x, t) \quad (\text{A.1})$$

in a 1D periodic domain  $[0, L]$  satisfies:

$$\partial_t \langle \xi \rangle = 0, \quad (\text{A.2})$$

with  $\langle \dots \rangle = \int_0^L dx [\dots]$  the spatial average. Note that  $\langle S \rangle = 0$  is a solvability condition for the system A.1, since  $\langle \nabla^2 \rangle = 0$ .

The formal proof begins by considering an augmented equation,

$$\partial_t \hat{\xi} = \frac{1}{\epsilon} [\nabla^2 \hat{\xi} - S]. \quad (\text{A.3})$$

The solution to this equation has the property that:

$$\lim_{\epsilon \rightarrow 0} \hat{\xi} \rightarrow \xi, \quad (\text{A.4})$$

i.e.,  $\xi$  is the quasi-static limit of  $\hat{\xi}$ . Applying the spatial average operator to Eq. A.3, and using the solvability condition, we find:

$$\partial_t \langle \hat{\xi} \rangle = 0.$$

Equation A.2 follows by taking the limit  $\epsilon \rightarrow 0$ .

## Appendix B. Magnetic field scattering formulas for exact conservation of particle canonical momenta

We begin with Eq. 39,

$$\frac{v_p^{\nu+1} - v_p^\nu}{\Delta \tau^\nu} = -\frac{q_p}{m_p} \sum_i \frac{A_i^{\nu+1} S_l(x_p^{\nu+1} - x_i) - A_i^\nu S_l(x_p^\nu - x_i)}{\Delta \tau^\nu}. \quad (\text{B.1})$$

We consider second-order splines ( $l = 2$ ). The analysis below can be extended to higher-order splines, if needed, by keeping more terms in the expansion. Taylor-expanding the  $l = 2$  shape functions at  $x_{p,i}^{\nu+1/2} \equiv (x_p^{\nu+1/2} - x_i)$ , we find:

$$\begin{aligned} S_2(x_p^{\nu+1} - x_i) &= S_2(x_{p,i}^{\nu+1/2}) + (x_p^{\nu+1} - x_p^{\nu+1/2}) \left. \frac{\partial S_2}{\partial x_p} \right|_{x_{p,i}^{\nu+1/2}} + \frac{(x_p^{\nu+1} - x_p^{\nu+1/2})^2}{2} \left. \frac{\partial^2 S_2}{\partial x_p^2} \right|_{x_{p,i}^{\nu+1/2}}, \\ S_2(x_p^\nu - x_i) &= S_2(x_{p,i}^{\nu+1/2}) + (x_p^\nu - x_p^{\nu+1/2}) \left. \frac{\partial S_2}{\partial x_p} \right|_{x_{p,i}^{\nu+1/2}} + \frac{(x_p^\nu - x_p^{\nu+1/2})^2}{2} \left. \frac{\partial^2 S_2}{\partial x_p^2} \right|_{x_{p,i}^{\nu+1/2}}. \end{aligned}$$

No higher-order terms are present for  $l = 2$ . Introducing these results into Eq. B.1, we find:

$$\begin{aligned} \frac{v_p^{\nu+1} - v_p^\nu}{\Delta\tau} &= \frac{q_p}{m_p} \sum_i \left[ -\frac{A_i^{\nu+1} - A_i^\nu}{\Delta\tau} S_2(x_p^{\nu+1/2} - x_i) \right] \\ &- v_{x,p}^{\nu+1/2} \sum_i \left[ A_i^{\nu+1/2} \frac{\partial S_2}{\partial x_p} \Big|_{x_{p,i}^{\nu+1/2}} + \frac{A_i^{\nu+1} - A_i^\nu}{8} (x_p^{\nu+1} - x_p^\nu) \frac{\partial^2 S_2}{\partial x_p^2} \Big|_{x_{p,i}^{\nu+1/2}} \right]. \end{aligned}$$

Noting that, within a macro-step:

$$-\frac{A_i^{\nu+1} - A_i^\nu}{\Delta\tau} = -\frac{A_i^{\nu+1} - A_i^\nu}{\Delta t} = E_i,$$

and comparing the velocity update above with Eq. 22 (discretized at  $\nu + 1/2$ ), the definition of the magnetic field at the particle position follows as:

$$B_{z,p}^{\nu+1/2} \equiv \sum_i \left[ A_{y,i}^{\nu+1/2} \frac{\partial S_2}{\partial x_p} \Big|_{x_{p,i}^{\nu+1/2}} + \frac{A_{y,i}^{\nu+1} - A_{y,i}^\nu}{8} (x_p^{\nu+1} - x_p^\nu) \frac{\partial^2 S_2}{\partial x_p^2} \Big|_{x_{p,i}^{\nu+1/2}} \right]. \quad (\text{B.2})$$

Here [1]:

$$\begin{aligned} \frac{\partial S_2}{\partial x_p} \Big|_{x_{p,i}^{\nu+1/2}} &= -\frac{\partial S_2}{\partial x} \Big|_{x_{p,i}^{\nu+1/2}} = -\frac{S_1(x_{i+1/2} - x_p^{\nu+1/2}) - S_1(x_{i-1/2} - x_p^{\nu+1/2})}{\Delta x}, \\ \frac{\partial^2 S_2}{\partial x_p^2} \Big|_{x_{p,i}^{\nu+1/2}} &= \frac{\partial^2 S_2}{\partial x^2} \Big|_{x_{p,i}^{\nu+1/2}} = \begin{cases} 1, & i = i_p - 1 \\ -2, & i = i_p \\ 1, & i = i_p + 1 \\ 0, & \text{else} \end{cases}, \end{aligned}$$

with  $i_p$  indicating the cell location of particle  $p$ . With periodic boundary conditions, the first term on the right hand side can be written as:

$$\sum_i A_{y,i}^{\nu+1/2} \frac{\partial S_2}{\partial x_p} \Big|_{x_{p,i}^{\nu+1/2}} = \sum_i \left[ \frac{A_{y,i+1}^{\nu+1/2} - A_{y,i}^{\nu+1/2}}{\Delta x} S_1(x_{i+1/2} - x_p^{\nu+1/2}) \right],$$

which corresponds to the standard scattering formula for the magnetic field at the particle position from a vector potential. The second term on the right-hand-side of Eq. B.2 can be written as:

$$\sum_i \frac{A_{y,i}^{\nu+1} - A_{y,i}^\nu}{8} (x_p^{\nu+1} - x_p^\nu) \frac{\partial^2 S_2}{\partial x_p^2} \Big|_{x_{p,i}^{\nu+1/2}} = \frac{\Delta A_{y,i_p-1}^{\nu+1/2} - 2\Delta A_{y,i_p}^{\nu+1/2} + \Delta A_{y,i_p+1}^{\nu+1/2}}{8\Delta x^2} (x_p^{\nu+1} - x_p^\nu),$$

where  $\Delta A^{\nu+1/2} = A^{\nu+1} - A^\nu$ . This additional term is a truncation error correction of  $\mathcal{O}[(\Delta\tau^\nu)^2]$ , which ensures exact canonical conservation for second-order shape functions ( $l = 2$ ). A similar prescription can be found for  $B_{y,p}$  from the conservation of  $p_z$ :

$$B_{y,p}^{\nu+1/2} = -\sum_i \left[ A_{z,i}^{\nu+1/2} \frac{\partial S_2}{\partial x_p} \Big|_{x_{p,i}^{\nu+1/2}} \right] - \frac{\Delta A_{z,i_p-1}^{\nu+1/2} - 2\Delta A_{z,i_p}^{\nu+1/2} + \Delta A_{z,i_p+1}^{\nu+1/2}}{8\Delta x^2} (x_p^{\nu+1} - x_p^\nu).$$

In our context, since the vector potential is periodic, a constant external magnetic field component (if it exists) cannot be captured, and needs to be added explicitly. This can be readily done by adding the corresponding constant magnetic field components to the scattering formulas above.

The contribution of the constant magnetic field to the canonical momenta must also be explicitly taken into account when diagnosing their conservation in a periodic domain. This can be done as follows. For a constant magnetic field  $\mathbf{B}_0 = (B_{0x}, B_{0y}, B_{0z})$ , the change in  $A_y$  and  $A_z$  (recall  $A_x$  must remain constant to enforce  $\nabla \cdot \mathbf{A} = 0$ ) over a substep along a particle orbit is given by:

$$A_{y,p}^{\nu+1} - A_{y,p}^{\nu} = B_{0z} \Delta x_p^{\nu} - B_{0x} \Delta z_p^{\nu} ; A_{z,p}^{\nu+1} - A_{z,p}^{\nu} = B_{0x} \Delta y_p^{\nu} - B_{0y} \Delta x_p^{\nu},$$

where  $(\Delta x_p^{\nu}, \Delta y_p^{\nu}, \Delta z_p^{\nu}) = (v_{x,p}, v_{y,p}, v_{z,p})^{\nu+1/2} \Delta \tau^{\nu}$ .

## Acknowledgments

The authors would like to acknowledge useful conversations with D. A. Knoll, W. Daughton, and the rest of CoCoMans team. This work was sponsored by the Los Alamos National Laboratory (LANL) Directed Research and Development Program. This work was performed under the auspices of the National Nuclear Security Administration of the U.S. Department of Energy at Los Alamos National Laboratory, managed by LANS, LLC under contract DE-AC52-06NA25396.

## References

- [1] C. K. Birdsall and A. B. Langdon, *Plasma Physics via Computer Simulation*. New York: McGraw-Hill, 2005.
- [2] R. W. Hockney and J. W. Eastwood, *Computer Simulation Using Particles*. Bristol, UK: Taylor & Francis, Inc, 1988.
- [3] B. B. Godfrey, “Numerical Cherenkov instabilities in electromagnetic particle codes,” *Journal of Computational Physics*, vol. 15, no. 4, pp. 504–521, 1974.
- [4] A. B. Langdon, “Some electromagnetic plasma simulation methods and their noise properties,” *Physics of Fluids*, vol. 15, p. 1149, 1972.
- [5] R. J. Mason, “Implicit moment particle simulation of plasmas,” *J. Comput. Phys.*, vol. 41, no. 2, pp. 233 – 244, 1981.
- [6] J. Denavit, “Time-filtering particle simulations with  $\omega_{pe}\Delta t \gg 1$ ,” *J. Comput. Phys.*, vol. 42, no. 2, pp. 337 – 366, 1981.
- [7] J. U. Brackbill and D. W. Forslund, “An implicit method for electromagnetic plasma simulation in two dimensions,” *Journal of Computational Physics*, vol. 46, p. 271, 1982.
- [8] H. Vu and J. Brackbill, “CELEST1D: an implicit, fully kinetic model for low-frequency, electromagnetic plasma simulation,” *Comput. Phys. Commun.*, vol. 69, p. 253, 1992.
- [9] A. Friedman, A. B. Langdon, and B. I. Cohen, “A direct method for implicit particle-in-cell simulation,” *Comments on plasma physics and controlled fusion*, vol. 6, no. 6, pp. 225 – 36, 1981.
- [10] B. I. Cohen, A. B. Langdon, and A. Friedman, “Implicit time integration for plasma simulation,” *J. Comput. Phys.*, vol. 46, no. 1, pp. 15 – 38, 1982.
- [11] A. B. Langdon, B. I. Cohen, and A. Friedman, “Direct implicit large time-step particle simulation of plasmas,” *J. Comput. Phys.*, vol. 51, no. 1, pp. 107 – 38, 1983.
- [12] D. C. Barnes, T. Kamimura, J. N. Leboeuf, and T. Tajima, “Implicit particle simulation of magnetized plasmas,” *J. Comput. Phys.*, vol. 52, no. 3, pp. 480 – 502, 1983.
- [13] J. Brackbill and D. Forslund, “Simulation of low-frequency electromagnetic phenomena in plasmas,” in *Multiple time scales* (J. U. Brackbill and B. I. Cohen, eds.), Academic Press, 1985.
- [14] A. B. Langdon and D. C. Barnes, “Direct implicit plasma simulation,” in *Multiple time scales* (J. U. Brackbill and B. I. Cohen, eds.), pp. 335–375, Academic Press, New York, 1985.
- [15] B. I. Cohen, “Multiple time-scale methods in particle simulations of plasma,” *Particle Accelerators*, vol. 19, pp. 227–236, 1986.

- [16] R. J. Mason, “An electromagnetic field algorithm for 2d implicit plasma simulation,” *Journal of Computational Physics*, vol. 71, no. 2, pp. 429–473, 1987.
- [17] D. W. Hewett and A. B. Langdon, “Electromagnetic direct implicit plasma simulation,” *J. Comput. Phys.*, vol. 72, no. 1, pp. 121 – 55, 1987.
- [18] A. Friedman, “A second-order implicit particle mover with adjustable damping,” *Journal of Computational Physics*, vol. 90, no. 2, pp. 292–312, 1990.
- [19] T. Kamimura, E. Montalvo, D. C. Barnes, J. N. Leboeuf, and T. Tajima, “Implicit particle simulation of electromagnetic plasma phenomena,” vol. 100, no. 1, pp. 77–90, 1992.
- [20] G. Lapenta and J. Brackbill, “CELESTE 3D: Implicit adaptive grid plasma simulation,” in *International School/Symposium for Space Simulation*, (Kyoto, Japan), March 13-19 1997.
- [21] M. Gibbons and D. Hewett, “The Darwin Direct Implicit Particle-in-Cell (DADIPIIC) method for simulation of low frequency plasma phenomena,” *Journal of Computational Physics*, vol. 120, pp. 231–247, 1995.
- [22] B. I. Cohen, A. B. Langdon, D. W. Hewett, and R. J. Procassini, “Performance and optimization of direct implicit particle simulation,” *J. Comput. Phys.*, vol. 81, no. 1, pp. 151 – 168, 1989.
- [23] S. Markidis and G. Lapenta, “The energy conserving particle-in-cell method,” *Journal of Computational Physics*, vol. 230, no. 18, pp. 7037–7052, 2011.
- [24] C. G. Darwin, “The dynamical motions of charged particles,” *The London, Edinburgh, and Dublin Philosophical Magazine and Journal of Science*, vol. 39, no. 233, pp. 537–551, 1920.
- [25] A. Hasegawa and H. Okuda, “One-dimensional plasma model in the presence of a magnetic field,” *Physics of Fluids*, vol. 11, p. 1995, 1968.
- [26] A. N. Kaufman and P. S. Rostler, “The Darwin model as a tool for electromagnetic plasma simulation,” *Physics of Fluids*, vol. 14, p. 446, 1971.
- [27] T. B. Krause, A. Apte, and P. Morrison, “A unified approach to the Darwin approximation,” *Physics of Plasmas*, vol. 14, p. 102112, 2007.
- [28] C. W. Nielson and H. R. Lewis, “Particle-code models in the nonradiative limit,” *Methods in Computational Physics*, vol. 16, pp. 367–388, 1976.
- [29] J. Busnardo-Neto, P. Pritchett, A. Lin, and J. Dawson, “A self-consistent magnetostatic particle code for numerical simulation of plasmas,” *Journal of Computational Physics*, vol. 23, no. 3, pp. 300–312, 1977.

- [30] J. Byers, B. Cohen, W. Condit, and J. Hanson, “Hybrid simulations of quasineutral phenomena in magnetized plasma,” *Journal of Computational Physics*, vol. 27, no. 3, pp. 363–396, 1978.
- [31] D. Hewett, “Low-frequency electromagnetic (Darwin) applications in plasma simulation,” *Computer physics communications*, vol. 84, no. 1, pp. 243–277, 1994.
- [32] E. Sonnendrücker, J. J. Ambrosiano, and S. T. Brandon, “A finite element formulation of the Darwin PIC model for use on unstructured grids,” *Journal of Computational Physics*, vol. 121, no. 2, pp. 281–297, 1995.
- [33] W. Lee, H. Qin, and R. C. Davidson, “Nonlinear perturbative electromagnetic (Darwin) particle simulation of high intensity beams,” *Nuclear Instruments and Methods in Physics Research Section A: Accelerators, Spectrometers, Detectors and Associated Equipment*, vol. 464, no. 1, pp. 465–469, 2001.
- [34] T. Taguchi, T. Antonsen Jr, and K. Mima, “Study of hot electron beam transport in high density plasma using 3D hybrid-Darwin code,” *Computer physics communications*, vol. 164, no. 1, pp. 269–278, 2004.
- [35] L. V. Borodachev, I. Mingalev, and O. Mingalev, “The numerical approximation of discrete Vlasov-Darwin model based on the optimal reformulation of field equations,” *Matematicheskoe Modelirovanie*, vol. 18, no. 11, pp. 117–125, 2006.
- [36] D. Eremin, T. Hemke, R. P. Brinkmann, and T. Mussenbrock, “Simulations of electromagnetic effects in high-frequency capacitively coupled discharges using the Darwin approximation,” *Journal of Physics D: Applied Physics*, vol. 46, no. 8, p. 084017, 2013.
- [37] H. Weitzner and W. S. Lawson, “Boundary conditions for the Darwin model,” *Physics of Fluids B: Plasma Physics*, vol. 1, p. 1953, 1989.
- [38] P. Degond and P.-A. Raviart, “An analysis of the Darwin model of approximation to Maxwell’s equations,” *Forum Math*, vol. 4, no. 4, pp. 13–44, 1992.
- [39] G. Chen, L. Chacón, and D. C. Barnes, “An energy- and charge-conserving, implicit, electrostatic particle-in-cell algorithm,” *Journal of Computational Physics*, vol. 230, pp. 7018–7036, 2011.
- [40] W. Taitano, D. Knoll, L. Chacón, and G. Chen, “Development of a consistent and stable fully implicit moment method for Vlasov-Ampère Particle-in-cell (PIC) system,” *SIAM J. Sci. Comput.*, 2013. In press.
- [41] B. Cohen, “Orbit averaging and subcycling in particle simulation of plasmas,” in *Multiple Time Scales*, Academic Press, 1985.
- [42] D. W. Hewett, “Elimination of electromagnetic radiation in plasma simulation: The Darwin or magnetoinductive approximation,” *Space Science Reviews*, vol. 42, pp. 29–40, 1985.

- [43] P.-A. Raviart and E. Sonnendrücker, “A hierarchy of approximate models for the Maxwell equations,” *Numerische Mathematik*, vol. 73, no. 3, pp. 329–372, 1996.
- [44] G. Chen and L. Chacón, “An analytical particle mover for the charge-and energy-conserving, nonlinearly implicit, electrostatic particle-in-cell algorithm,” *Journal of Computational Physics*, vol. 247, pp. 79–87, 2013.
- [45] L. Chacón, G. Chen, and D. C. Barnes, “A charge- and energy-conserving implicit, electrostatic particle-in-cell algorithm on mapped computational meshes,” *Journal of Computational Physics*, 2012. accepted.
- [46] E. Weibel, “Spontaneously growing transverse waves in a plasma due to an anisotropic velocity distribution,” *Physical Review Letters*, vol. 2, no. 3, pp. 83–84, 1959.
- [47] B. Fried, “Mechanism for instability of transverse plasma waves,” *Physics of Fluids*, vol. 2, p. 337, 1959.
- [48] J. Williamson, “Initial particle distributions for simulated plasma,” *Journal of Computational Physics*, vol. 8, no. 2, pp. 258–267, 1971.
- [49] N. A. Krall and A. W. Trivelpiece, *Principles of plasma physics*. International Student Edition-International Series in Pure and Applied Physics, Tokyo: McGraw-Hill Kogakusha, 1973.
- [50] C. Chang, H. Wong, and C. Wu, “Electromagnetic instabilities attributed to a cross-field ion drift,” *Physical review letters*, vol. 65, no. 9, pp. 1104–1107, 1990.
- [51] L. Yin, D. Winske, W. Daughton, and K. Bowers, “Kinetic Alfvén waves and electron physics. I. Generation from ion-ion streaming,” *Physics of plasmas*, vol. 14, no. 6, pp. 062104–062104, 2007.
- [52] G. Chen, L. Chacon, C. A. Leibs, D. A. Knoll, and W. Taitano, “Fluid preconditioning for Newton-Krylov-based, fully implicit, electrostatic particle-in-cell simulations,” *Journal of computational physics (submitted)*, *arXiv preprint arXiv:1309.6243*, 2013.